Symmetry- and multiplet-resolved N 1s photoionization cross sections of the NO2 molecule

Symmetry- and multiplet-resolved N 1*s* photoionization cross sections of the NO_2 molecule

N. Saito,[1] D. Toffoli,[2] R. R. Lucchese,[2] M. Nagoshi,[3] A. De Fanis,[4] Y. Tamenori,[4] M. Oura,[5] H. Yamaoka,[5] M. Kitajima,[6] H. Tanaka,[6] U. Hergenhahn,[7,8] and K. Ueda[7,*]

[1]*NMIJ, National Institute of Advanced Industrial Science and Technology (AIST), Tsukuba 305-8568, Japan*
[2]*Department of Chemistry, Texas A&M University, College Station, Texas 77843-3255, USA*
[3]*Department of Material Science, Himeji Institute of Technology, Kamigori, Hyogo 678-1297, Japan*
[4]*Japan Synchrotron Radiation Research Institute, Sayo, Hyogo 679-5198, Japan*
[5]*RIKEN, Harima Institute, Sayo, Hyogo 679-5148, Japan*
[6]*Department of Physics, Sophia University, Tokyo 102-8554, Japan*
[7]*Institute of Multidisciplinary Research for Advanced Materials, Tohoku University, Sendai 980-8577, Japan*
[8]*Max-Planck-Institute for Plasma Physics, EURATOM Association, Boltzmannstrasse 2, 85748 Garching, Germany*

(Received 14 July 2004; published 30 December 2004)

We present a joint theoretical and experimental investigation of the N 1*s* photoionization of NO_2 in the shape resonance region. The theoretical calculations, based on a single-channel relaxed-core Hartree-Fock approximation, predict that the shape resonance appears only in the $A_1 \rightarrow B_2$ transition and that the shape resonance energy of the N $1s^{-1}\ ^1A_1$ channel is about 2.6 eV lower in kinetic energy than that of the N $1s^{-1}\ ^3A_1$ channel, suggesting that the potential for the $^1A_1$ channel is much more attractive than that for the $^3A_1$ channel. Symmetry-selected cross sections measured by means of a multiple-ion coincidence imaging prove that the shape resonance appears only in the $A_1 \rightarrow B_2$ transition, as predicted by the calculation. The experimental partial cross sections for the N $1s^{-1}\ ^1A_1$ and $^3A_1$ channels measured by means of conventional electron spectroscopy exhibit the shape-resonance maxima at photon energies of 416.3 and 415.9 eV, respectively, at corresponding kinetic energies of 3.0 and 3.3 eV, respectively, implying that the attractive potential for the $^1A_1$ channel is overestimated in the single-channel approximation. The possible role played by correlation effects on the *K*-shell ionization of NO_2 is discussed in terms of interchannel coupling between the main-line channels and, possibly, with additional excited target states.

DOI: 10.1103/PhysRevA.70.062724 PACS number(s): 33.80.Eh, 33.60.Fy, 33.20.Rm, 33.70.Ca

I. INTRODUCTION

Strong resonance features in *K*-shell absorption spectra of small molecules are usually described as the transition of a 1*s* electron to an unoccupied molecular valence-like orbital [1]. Another method which has been widely used to describe the resonances above the threshold, often called *shape resonances*, ascribes the resonant enhancement to the temporary trapping of the photoelectron by the angular momentum barrier, through which the electron eventually tunnels, emerging in the continuum [2,3]. Both extensive experimental and theoretical studies have been carried out for soft x-ray interactions with various molecules and these studies have been in many excellent critical reviews, such as the recent one by Piancastelli [4].

The present study is concerned with shape resonances which appear in the N 1*s* photoionization spectrum of NO_2. The photoabsorption spectra of NO_2 in the soft x-ray range reveal pronounced absorption peaks, which can be rationalized using single-particle theories [2,3], if one neglects the accompanying many-body effects, notably Auger processes. There is a substantial practical and fundamental need for quantitative spectroscopic information for NO_2 in the soft x-ray region of the electromagnetic spectrum, because of the role played by its trace constituents in the upper levels of the earth's atmosphere in the reaction leading to the depletion of the ozone layer [5,6]. The NO_2 molecule belongs to the C_{2v} point group in the ground state, the electronic configuration of which is

$$1b_2^2 1a_1^2 2a_1^2 3a_1^2 2b_2^2 4a_1^2 5a_1^2 3b_2^2 1b_1^2\ 1a_2^2 4b_2^2 6a_1^1\ 2b_1^0 7a_1^0 5b_2^0;\ ^2A_1. \tag{1}$$

The dipole allowed transition from the ground state in A_1 symmetry reaches the A_1, B_1, and B_2 symmetry states (see, for example, [7,8]). Figure 1 shows relations between the molecular orientation and the dipole moment for the excitation or ionization to the A_1, B_1, and B_2 states. There are a couple of characteristic points to be addressed. First, in the previous studies [8–10], the shape resonance in the N $1s^{-1}$ continuum state has been assigned to a promotion of the N $1s\ 2a_1$ electron to the unoccupied $5b_2^*$ molecular orbital. Thus, the shape resonance appears only in the B_2 symmetry continuum. Second, NO_2 is an open shell molecule and core ionization leads thus $^3A_1$ and $^1A_1$ core-hole states of NO_2^+, with a $2a_1^{-1}6a_1$ configuration. The attractive potential experienced by the escaping electron can be different for the $^1A_1$ and $^3A_1$ final states, possibly affecting the shape resonance energies. Furthermore, the photoionization channels are doubled with respect to a closed-shell case, with the additional possibility of interchannel coupling between them.

We have carried out theoretical calculations on the N 1*s* photoionization of NO_2, in the framework of the single-channel relaxed-core Hartree-Fock (SCRCHF) approximation [11–14], and using multiplet-specific potentials, for the

*Electronic address: ueda@tagen.tohoku.ac.jp

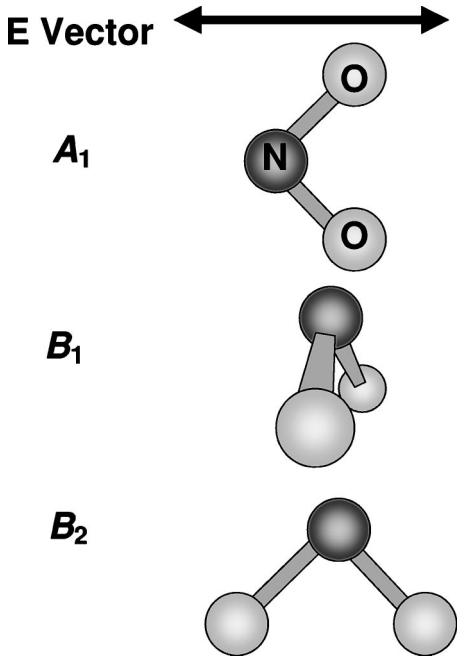

FIG. 1. Relations between the molecular orientation and the E vector when the molecule is ionized into A_1, B_1, and B_2 states.

determination of the singlet and triplet partial cross sections and asymmetry parameters profiles. The theory confirmed that the shape resonance appears only in the B_2 symmetry continuum. Furthermore, the theory predicts that the shape resonance energy exhibits strong term dependence, suggesting a much more attractive effective potential in the $^1A_1$ channel than in the $^1A_1$ channel.

Using these predictions as a guide, we have carried out two different experiments, multiple-ion coincidence imaging [15–19] and core-level photoelectron spectroscopy [20–22]. The former allows us to measure the symmetry-selected partial cross sections and confirms that the shape resonance appears only in the B_2 symmetry continuum. The latter allows us to measure the multiplet resolved partial photoabsorption cross sections. The result indicates that the potential in the $^1A_1$ channel is more attractive than in the $^3A_1$ channel but not as attractive as predicted in theory. We will therefore discuss how the inclusion of correlation effects, which are not explicitly included in our theoretical approach, can potentially alter the single-particle picture of the K-shell ionization of NO_2 which emerges from our calculations.

The next section describes our theoretical method and computational details. Section III describes our experimental methods and procedures. In Sec. IV, we compare the theoretical and experimental results and discuss them. Section V is a summary.

II. THEORETICAL

A. Method

The N 1s inner shell photoionization of the NO_2 molecule was studied within the SCRCHF approximation. Since the basics of the SCRCHF theoretical method employed are extensively covered in the literature [11–14], here we only sketch the general features. The essential quantities in the calculation of molecular photoionization cross section and asymmetry parameters are the "length" and "velocity" forms of the dipole transition matrix elements,

$$I^{(L)}_{\vec{k},\hat{n}} = (k)^{1/2}\langle \Psi_i | \vec{r}\cdot\hat{n} | \Psi^{(-)}_{f,\vec{k}} \rangle \tag{2}$$

and

$$I^{(V)}_{\vec{k},\hat{n}} = \frac{(k)^{1/2}}{E}\langle \Psi_i | \nabla \cdot \hat{n} | \Psi^{(-)}_{f,\vec{k}} \rangle, \tag{3}$$

respectively. In Eqs. (2) and (3), Ψ_i is the target ground state wave function, $\Psi^{(-)}_{f,\vec{k}}$ is the final-state wave function, E is the photon energy, $\vec{k}$ is the photoelectron momentum, and $\hat{n}$ is a unit vector in the direction of polarization of the light. In our SCRCHF approximation, both the initial- and final-state electronic wave functions are represented by single spin- and symmetry-adapted configuration state functions constructed using a common set of molecular orbitals (MOs). Specifically, we have used the HF MOs of the final ion target states, with a fixed hole in the $2a_1$ N 1s orbital (*vide infra*). This procedure attempts to capture some of the effects arising from the relaxation of the ionic core, with the advantage of avoiding the nonorthogonality problem which occurs when the initial and final states use different orbital sets [23,24]. In this respect we note that similar procedures, while employing MO sets obtained by using the Slater's transition-state approximation [25], have been widely used in recent years when dealing with inner-shell excitation and photoionization processes [26–31]. Independent of the choice of the set of MOs used to build the initial and final scattering states of the system, in the SCHF approximation the scattering problem is reduced to the solution of a Schrödinger-type equation for the unbound photoelectron orbital:

$$\left[-\frac{1}{2}\nabla^2 + V_{N-1}(\vec{r},\vec{R}) + \frac{k^2}{2} \right] \phi^{(-)}_{\vec{k}}(\vec{r}) = 0. \tag{4}$$

In Eq. (4), V_{N-1} is the static-exchange (SE) potential of the molecular ion and $\phi^{(-)}_{\vec{k}}(\vec{r})$ satisfies the appropriate scattering boundary conditions. In our implementation we recast the differential equation (4) together with the boundary conditions to the corresponding integral equation (the Lippmann-Schwinger equation) by using the appropriate Green function. The Lippmann-Schwinger equation is solved by employing the single center expansion technique [13] together with an iterative procedure based on the Schwinger variational principle and Padé approximants [11]. Full advantage is taken of the symmetry of the nonlinear target (C_{2v} in the present case), by using symmetry-adapted spherical harmonics, which transform as the various irreducible representations of the molecular point group [13]. Finally, the photoelectron angular distributions for the final target states N $1s^{-1}$ $^1A_1$ and $^3A_1$ of NO_2^+, of the form

$$\frac{d\sigma_i^{(L,V)}}{d\Omega_{\hat{k}}} = \frac{\sigma_i^{(L,V)}}{4\pi}\{1 + \beta_i^{(L,V)} P_2[\cos(\theta)]\}, \quad (5)$$

where $i = {}^1A_1$ or ${}^3A_1$, can be expressed in terms of the partial-wave components of the dynamical coefficients $I_{\vec{k},\hat{n}}^{(L,V)}$ of Eqs. (2) and (3) using standard expressions [11]. In the calculations reported here we will present results in the mixed form of the dipole operator which is known to satisfy the Thomas-Reiche-Kuhn sum rule [32].

While our present implementation of the close-coupling scattering equations does not allow for the mixing of different electronic target states, essentially restricting our analysis to a one-electron picture of the phenomenon, the coupling of the continuum partial-wave channels induced by the anisotropic molecular potential is fully accounted for, greatly improving the theoretical description of the scattering process over the past investigations [8,9] which based their analysis on the crude muffin-tin approximation for the interaction potential, usually assumed in the multiple-scattering method [33,34]. It is also worth noting that the past theoretical treatment of the scattering process [8,9] did not take into account the two possible spin-multiplicities of the final ionic states, giving results referring only to the ${}^3A_1$ N $1s^{-1}$ ionic state. Lastly, as will be outlined in the computational section, the strong relaxation effects that inevitably follow the ionization of the strongly localized N 1*s* core orbital are modeled with a careful choice of the molecular orbital set used in the construction of the final target states.

Furthermore, electron scattering resonances in specific continuum channels have been analyzed by using the adiabatic static model exchange (ASME) method [35], which employs a local approximation to the HF exchange term and solves the resulting scattering equations in a set of "adiabatic" angular functions. In the ASME method, the resonant energies are determined by locating the poles of the scattering matrix on the unphysical sheet of the complex plane [36] and the corresponding wave function is then extracted and analyzed. The ASME method has been widely used in recent years by our group [12,35,37,38] for the characterization of shape resonances in terms of "dynamical" trapping of high-*l* partial waves in the molecular range of the effective scattering potential. An interpretation of these resonant processes as one-electron transitions to virtual antibonding MOs can be drawn from the comparison between the continuum ASME orbitals and virtual molecular orbitals obtained from minimum basis set (MBS) calculations.

B. Computational details

For the two NO_2^+ N $1s^{-1}$ ion target states, the photoelectron wave functions are obtained by using the SE potential constructed from the self-consistent field (SCF) orbitals of the corresponding ion states. In the SCF calculations we have used the augmented correlation-consistent polarized valence triple zeta (aug-cc-pVTZ) basis set included in the MOLPRO [39] suite of programs. The SCF total energies obtained with this basis set were −188.841 907 a.u. and −188.870 877 a.u. for the ${}^1A_1$ and ${}^3A_1$ N $1s^{-1}$ ion states respectively, at the NO_2 equilibrium geometry of the ground state [R(N-O)=1.19455 Å and ∠(O-N-O)=133.851° from Ref. [40]]. At the same geometry the (aug-cc-pVTZ) SCF energy of the ground state is −204.105 612 a.u., giving a singlet-triplet spacing of about 0.78 eV, which compares remarkably well with the experimental XPS result of 0.70 eV [41].

As a preliminary to this work we have studied the effects of the degree of core relaxation on the shape resonant cross section (total symmetry ${}^2B_2$) in order to select the most suitable sets of MOs for the construction of the initial *N*-electron and final $(N-1)$-electron states. We first attempted to study the N *K*-shell ionization of NO_2 by the simpler frozen-core HF (FCHF) approximation [11], where the neutral-molecule ground-state SCF orbitals are assumed for both the initial and final ionic states. However, the unscreened FCHF scattering potential proved too attractive, which caused a shift of the resonance positions below the ionization thresholds. We then tried to model the restructuring of the molecular core following the ionization by using MO sets obtained from a multi-configuration SCF calculation with selected single-hole configurations included. Again we found that the resulting V_{N-1} potential was too attractive, especially in the N $1s^{-1}$ $({}^1A_1)$ scattering channel. These preliminary results indicated that the best approach would be to include relaxation effects using continuum orbitals determined in the field of the completely relaxed ion core. Although this assumption is not rigorous, early applications to atomic and molecular photoionization have shown that this is quite reasonable, usually giving relaxed-core cross sections which compare favorably with the experiment, after a typical shift of a few eV to lower photon energies [23]. As a result of the excessive screening of the N $1s^{-1}$ hole, we have shifted our results by 5.5 eV to lower photon energies in order to compare with the experiment. Photoelectron kinetic energies were converted to photon energies, using the experimental values for the ionization potentials reported in the literature [8], namely 412.6 and 413.3 eV for the ${}^3A_1$ and ${}^1A_1$ N $1s^{-1}$ target states, respectively.

Our expansion for the molecular orbitals and for the scattering wave functions included partial wave up to $l_{max}=30$. With this truncation, the largest error in the normalization of the molecular orbitals was 1.4% for the $1a_1$ and $1b_2$ orbitals (1*s* on the oxygen atoms).

III. EXPERIMENTAL

The experiments were carried out on the c branch of the soft x-ray photochemistry beamline 27SU [42,43] at SPring-8. A figure-8 undulator of this beamline provides linearly polarized light, whose electric vector is horizontal for the first-order harmonic light and vertical for the 0.5th-order harmonic light [44]. With acceptance angles employed in the present experiments, the degree of light polarization is almost perfect on the beam axis [45]. The monochromator is of Hettrick type [46,47]. It has three exchangeable varied line-spacing plane gratings and covers the photon energy region from 150 to 2500 eV [48]. The photon bandwidth used for the present experiment was about 140 meV at the photon energy of 410 eV. We carried out two different types of ex-

periments, a multiple-ion-coincidence momentum imaging [15–19] and angle-resolved core-level photoemission spectroscopy [20–22].

Our multiple-ion-coincidence momentum imaging is based on a measurement of the time-of-flight (TOF) of the positively charged particles with a position-sensitive ion detector [15–19]. Photoionization of the N 1*s* orbital generally leads to the creation of doubly or triply charged molecules, which fragment as a result of the ionization. In our study, we have selected reaction channels in which the molecule fully fragmented into singly charged atomic ions, $N^+ + O^+ + O^+$, which were then detected in coincidence. Measurements of the position and the arrival time on the detector, (x,y,t), of all the three ions, N^+, O^+, and O^+, in coincidence allowed us to extract information about the linear momentum (p_x,p_y,p_z) of each ion without any ambiguity and thus to resolve the symmetry species, A_1, B_1, and B_2, of the photoionized continuum states in the NO_2 molecule, as described in detail in the following subsection.

The NO_2 sample gas was introduced in the form of a supersonic jet and crossed the photon beam perpendicularly. The photon beam was focused to a size of less than 0.5 mm in height and 0.2 mm in width. The TOF axis was fixed perpendicularly to both the light beam and the supersonic jet. The length of the acceleration regions for the ion TOF spectrometer was 21.6 mm and no field free drift region was equipped. Ions were extracted with a static extraction field of about 1.1 V/mm and were detected by a multi-channel plate (MCP) of 80 mm effective diameter, followed by a two-dimensional square-type delay-line anode (DLD-80, manufactured by RoentDek [49]). Electrons were detected by another MCP of 80 mm effective diameter placed at the opposite end of the accelerating region, followed by a hexagonal-type delay-line anode (HEX-80, manufactured by RoentDek [49]) with an acceleration region of 32.9 mm and a drift region of 66.7 mm. A uniform magnetic field was superimposed to the spectrometer by a set of Helmholtz coils outside the vacuum chamber. The magnetic field was zero near the N 1*s* ionization threshold or 5 G for higher photoelectron energies. Under these conditions all the N 1*s* photoelectrons ejected in 4π sr were driven onto the MCP.

TOFs of ions and electrons were measured with respect to the bunch marker of the synchrotron radiation source. The storage ring was operated in a 203-bunch mode, which corresponded to a bunch separation of 23.6 ns. The data were recorded when at least one electron and three ions were detected in coincidence. The measurements were performed for the vertical direction of the photon polarization vector (*E* vector). In the experiment, the N 1*s* photoelectrons were recorded in coincidence with three ions. The coincident photoelectron spectra were, however, severely contaminated by the overlap of the low-energy Auger electron spectra, because the three-ion coincidence selects the channels which emit the low energy second-step Auger electron from the Auger final state (Auger cascades) as well as the channels which emit two Auger electrons from a single core-hole state (double Auger) and thus the low-energy electron coincident with three ions can be not only the N 1*s* photoelectron but also the low-energy Auger electron. Rather poor momentum resolution for the electrons and insufficient quadruple coincidence count rates, together with the overlap between the photoelectron and the low-energy Auger electron, prevented us from determining the multiplet-resolved partial cross sections for the $^3A_1$ and $^1A_1$ channels from the present coincidence experiment.

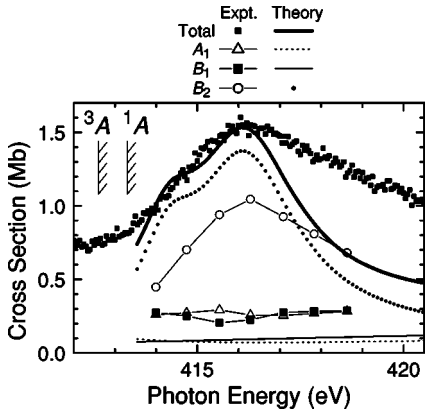

FIG. 2. Symmetry-selected photoabsorption spectra and total ion yield of NO_2 above the N 1*s* ionization threshold, together with theoretical symmetry-selected partial cross sections. The statistic error for the experimental data is less than the symbol size. The total ion yield intensity is normalized to the theoretical total intensity at 416 eV.

Angle-resolved core-level photoemission spectroscopy was employed to obtain the multiplet-resolved partial photoabsorption cross sections for the $^3A_1$ and $^1A_1$ channels. The electron spectroscopy apparatus consisted of a Gammadata-Scienta SES-2002 hemispherical electron energy analyzer with a gas cell and a differentially pumped chamber; the lens axis was fixed in the horizontal direction and the photon beam was parallel to the entrance slit [50]. The analyzer was operated at a pass energy of 5 eV and a slit of 4 mm, resulting in an electron energy resolution of about 63 meV. Angle-resolved photoelectron spectra were measured by switching the direction of the photon polarization vector from horizontal to vertical and vice versa [44]. The transmission function of the analyzer was obtained by recording the Ne 1*s* photoelectron spectrum in the kinetic energy region of interest and in agreement with a more extended calibration of the analyzer transmission to be discussed in a subsequent publication.

IV. RESULTS AND DISCUSSION

A. Symmetry-selected partial cross sections

The theoretical symmetry-selected partial cross section curves are illustrated in Fig. 2. The theoretical profiles have been shifted by 5.5 eV to lower photon energy in order to reproduce the experimental position of the resonance.

A simple interpretation of the resonant states can be gained from the comparison between the continuum wave function calculated with the ASME method and virtual orbitals obtained from MBS calculations on the molecular ground state. Figure 3 shows the $5b_2$ virtual orbital as obtained from a HF/STO-3G calculation on NO_2 (upper panel) and the real part of the εb_2 resonant wave function for the triplet N $1s^{-1}$

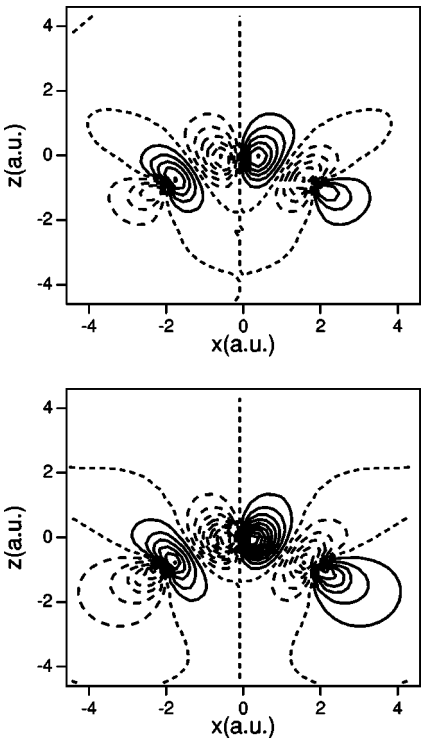

FIG. 3. Upper panel, $5b_2$ virtual orbital obtained from a MBS-SCF calculation on NO_2, where the dotted lines are nodes and the contours are separated by 0.05 a.u. Lower panel, the real part of the εb_2 resonant wave function for the triplet N $1s^{-1}$ scattering channel. The dotted lines are nodes and the contours are separated by 0.1 a.u.

scattering channel (lower panel). The strict similarity displayed by the two orbitals leads us to interpret the resonant state as a one-electron transition to the $5b_2^*$ virtual antibonding orbital, in agreement with the earlier works [8–10]. In addition, the analysis of the radial components of the ASME continuum wave function (not reported) suggests that the resonant states are predominantly *f* waves at large distances, in accord with past theoretical investigations [8,9].

In passing we note that the present results are very similar to the resonant state found in the low-energy electron scattering from NO_2 [51], once more highlighting the close connection existing between resonant states found in photoionization and electron scattering processes [52].

In order to derive the symmetry-selected partial cross sections from the triple-ion coincidence momentum imaging, the following data treatment is applied. Figure 1 shows relations between the *E* vector and the molecular orientation when the molecule is ionized into A_1, B_1, and B_2 states. The triple-ion coincidence momentum imaging allows us to extract the linear momenta of N^+, $p(N^+)$, and the oxygen fragments, $p(O_1^+)$ and $p(O_2^+)$. Note that the C_{2v} molecular axis coincides with $p(N^+)$ whereas the normal vector $\vec{n}$ of the molecular plane coincides with the vector product $p(O_1^+) \times p(O_2^+)$. Thus, we can define the orientation of the molecule and thus the transition symmetry for each event. The transition dipole moment for the $A_1 \rightarrow A_1$ transition is parallel to the C_{2v} molecular axis. Thus we have extracted the $A_1 \rightarrow A_1$ transition, selecting the events in which $p(N^+)$ is parallel to the *E* vector, with the angles between $p(N^+)$ and the *E* vector smaller than 20°. The transition dipole moment for the $A_1 \rightarrow B_1$ transition is perpendicular to the molecular plane. Thus, we have extracted the $A_1 \rightarrow B_1$ transition, selecting the events in which $p(O_1^+) \times p(O_2^+)$ is parallel to the *E* vector, with the angles between $p(O_1^+) \times p(O_2^+)$ and the *E* vector smaller than 20°. For the $A_1 \rightarrow B_2$ transition, the transition dipole moment is in the molecular plane and perpendicular to the C_{2v} molecular axis. Thus we have extracted the $A_1 \rightarrow B_2$ transition, selecting the events in which $p(O_1^+) - p(O_2^+)$ are parallel to the *E* vector, with the angles between $p(O_1^+) - p(O_2^+)$ and the *E* vector larger than 20°. The purity of A_1, B_1, and B_2 thus extracted are estimated to be better than 96%.

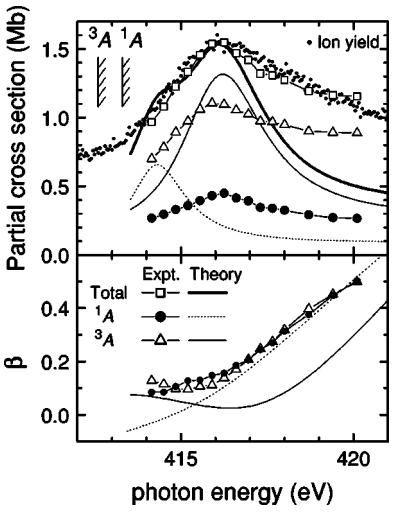

FIG. 4. Multiplet-resolved N 1*s* partial cross sections and asymmetry parameters of NO_2, as measured and as calculated. The error bar for the experimental β values is ±0.05.

From the extraction of the transition symmetry described above, we have determined the intensity ratios among the $A_1 \rightarrow A_1$, $A_1 \rightarrow B_1$, and $A_1 \rightarrow B_2$ transitions and decomposed the total cross section, represented by the total ion yield, into the symmetry-selected partial cross sections using these ratios. Figure 2 includes also the experimental symmetry-selected partial cross sections thus obtained for the $A_1 \rightarrow A_1$, $A_1 \rightarrow B_1$, and $A_1 \rightarrow B_2$ transitions, together with the total ion yield spectrum. The total ion yield spectrum is normalized to the maximum of the calculated cross section. One can see that the shape resonance appears only in the $A_1 \rightarrow B_2$ transition, as predicted and discussed above. The partial cross sections of the transitions to the A_1 and B_1 states show no enhancement around the shape resonance region: the measured cross sections are somewhat larger than the theoretical results.

B. Multiplet-resolved partial cross sections

The calculated $^1A_1$ and $^3A_1$ N $1s^{-1}$ partial cross sections are shown in Fig. 4. The theoretical profiles have been shifted by 5.5 eV to lower photon energy as in the case of Fig. 2. Then the shape resonance for the $^3A_1$ channel appears at a photon energy of 416.25 eV and for the $^1A_1$ channel is at

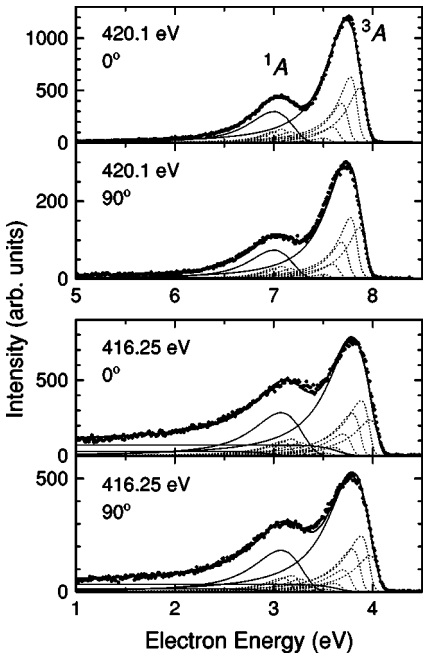

FIG. 5. Angle-resolved photoelectron spectra of NO_2 measured at the photon energies of 420.1 and 416.25 eV. The peaks at the lower and higher electron energies correspond to the $^1A_1$ and $^3A_1$ photoelectrons, respectively. The solid and dashed curves are the results of the fitting (see text).

a photon energy of 414.34 eV, which is lower than for the $^3A_1$ channel. The theoretical results thus suggest that the effective potential experienced by the photoelectron in the $^1A_1$ channel is much more attractive than that in the $^3A_1$ channel.

The calculated values of the asymmetry parameter β for the two channels are shown in the lower panel of Fig. 4. The β for the $^1A_1$ channel is negative at the threshold and increases as the photon energy increases, whereas the asymmetry parameter for the $^3A_1$ channel has a minimum at a photon energy of about 417 eV, overall reflecting the cross section results.

The following procedure was applied to extract the intensity ratios for the $^1A_1$ and $^3A_1$ photoelectrons. Figure 5 shows examples of angle-resolved photoelectron spectra of NO_2 measured at photon energies of 420.1 and 416.25 eV. First, a slanted baseline due to scattered electrons was subtracted and the correction for the transmission of the analyzer was made for all the spectra. Then, contributions from second step Auger transitions were subtracted: the spectrum recorded at 420.1 eV was used as a reference, which was subtracted from the spectra at all photon energies. Spectra in Fig. 5 correspond to the ones after these corrections. Then, we have fitted the spectra with two vibrational progressions corresponding to the $^1A_1$ and $^3A_1$ photoelectrons. Here a Poisson distribution for the vibrational components with a spacing of 90 meV was assumed. A PCI line shape by van der Straten *et al.* [53] with a constant natural width of 130 meV was employed for each vibrational component. The points in Fig. 5 are the experimental data. The dashed lines correspond to the vibrational components obtained by the curve fit and the two solid curves denote the sum over the vibrational components for $^1A_1$ and $^3A_1$. The curve fitted to the data points is the sum of these two solid curves. In order to obtain the spectral intensities for $^1A_1$ and $^3A_1$, the area of the fitted curves were integrated from $-\infty$ to the maximum kinetic energy is calculated. The partial cross section σ and asymmetry parameter β are obtained using the following equations:

$$\sigma = I(0°) + 2I(90°), \tag{6}$$

$$\beta = \frac{2[I(0°) - I(90°)]}{I(0°) + 2I(90°)}. \tag{7}$$

The resulting $^1A_1$ and $^3A_1$ N $1s^{-1}$ partial cross sections σ and asymmetry parameters β are included in Fig. 4. The experimentally obtained total cross section is in good agreement with the ion yield curve, suggesting that the correction of the transmission function for the photoelectron spectra is reasonable. The $^1A_1$ and $^3A_1$ N $1s^{-1}$ partial cross sections show maxima at the photon energies of 416.3 and 415.9 eV, respectively. Given that the ionization potentials for the $^1A_1$ and $^3A_1$ N $1s^{-1}$ states are 413.3 and 412.6 eV, respectively [41], the energy difference of the two multiplet thresholds thus is 0.7 eV, whereas the energy difference of the shape resonance for the two multiplet components is 0.4 eV. This means that the potential in the $^1A_1$ channel is somewhat more attractive than that in the $^3A_1$ channel. The agreement with theoretical prediction is, however, not completely satisfactory. The experimental β for the $^1A_1$ channel agrees well with the theoretical prediction, whereas the experimental β for the $^3A_1$ channel nearly coincides to that of the $^1A_1$ channel and exhibits deviation from the theoretical prediction.

The latter observation suggests that many-body effects, not explicitly included in our theoretical treatment, are likely to play an important role in the narrow energy region explored in the present study. Thus the more likely explanation for the discrepancies found between the measured and calculated σ and β is the neglected interchannel coupling. An example where the interchannel coupling proves important is the $5\sigma^{-1}$ photoionization from NO [54]. In that work it was indeed pointed out that strong multiplet-specific effects in the $5\sigma^{-1}$ photoionization did not show up in a multichannel treatment of the process: in a correlated treatment, a resonant feature does not always allow for an analysis in terms of isolated channels. This happens in instances when a single resonant state decays into different exit channels, as was found in NO [54].

The observation that interchannel coupling between two inner-shell open channels, whose thresholds are closely separated in energy, is responsible for a substantial redistribution and/or shift of intensity among the coupled channels, has been rather well documented in recent years, especially in the atomic case [55,56]. Thus, in the 3*d* photoionization from atomic xenon, it has been experimentally suggested [55] and soon thereafter theoretically demonstrated [56] that the interaction among photoionization channels from the members of a spin-orbit doublet produces a marked redistribution of intensity between the two main-line channels. The latter finding could at first suggest that similar correlation effects take place between the $^1A_1$ and $^3A_1$ exit channels in NO_2, whose energy separation of about 0.7 eV is determined by the ex-

change interaction. However, in the present case the existence of two separate resonances cannot be simply assumed, in contrast to the Xe case [55,56], since the resonant enhancements in the $^1A_1$ and $^3A_1$ exit channels are experimentally found to be very close in energy.

From the comparison between theory and experiment we can reasonably expect interchannel coupling effects to manifest themselves into two different and distinct ways, notably (a) there can be only a single resonant state with significant oscillator strength which decays into both the $^1A_1$ and $^3A_1$ channels (as found for example in the NO system [54]), indicating that interchannel coupling effects are of equal importance to the multiplet specific intrachannel interaction terms, or (b) there are possibly two strong resonances which accidentally happen to occur at roughly the same photon energy. In case (b) it is still reasonable to assume that interchannel coupling can potentially affect the distribution of oscillator strength between the two resonant continua, compared to a single-channel treatment, therefore in a manner similar to that found in Xe [55,56].

In order to shed some light to these open issues, we have determined the dipole transition moments for the two $2a_1 \rightarrow 5b_2^*$ transitions. Minimum basis set and improved virtual orbital (IVO) calculations have been shown in many instances to give a reasonable qualitative understanding of the location of the resonances [35,57]. We have therefore performed a minimum-basis restricted-active space (MB-RAS) calculation with the MOLPRO suite of programs [39] on the *N*-electron N $1s^{-1}$ core hole states of NO_2. Such a calculation is therefore expected to give qualitative insights about the mutual position and the one-particle nature of the *N*-electron resonances. The MB-RAS calculation gives two *N*-electron states which correspond to $2a_1 \rightarrow 5b_2^*$ excited states (although both of the states show strong mixing with higher excited configurations) and with appreciable oscillator strength. For the first state, the dominant $2a_1 \rightarrow 5b_2^*$ configuration shows the $2a_1$ and $6a_1$ orbitals singlet coupled and is predicted at a total energy of 421.07 eV. For the second state, the dominant $2a_1 \rightarrow 5b_2^*$ configuration shows the $2a_1$ and $6a_1$ orbitals triplet coupled with an excitation energy of 422.34 eV, with a singlet-triplet separation of about 1.3 eV. These theoretical findings thus suggest that, at variance with the NO case [54] there are likely two separate resonances in both the $^1A_1$ and $^3A_1$ channels whose mutual separation is found to be of roughly 1.3 eV in the MB-RAS calculation and 1.9 eV in the SE scattering calculations (2.0 and 2.6 eV, respectively, in the kinetic energy scale). Also note that both the calculations consistently predict a more attractive $^1A_1$ scattering potential compared to the $^3A_1$ one. The discrepancies between these theoretical values and the experimental one of 0.3 eV could then be ascribed partially to experimental uncertainties (the estimated error affecting the energy separation of the two resonant features is determined to be about 0.4 eV) and to the neglect of interchannel coupling between the two $^1A_1$ and $^3A_1$ exit channels and, possibly, coupling with additional excited target states (i.e., shake-up states).

V. CONCLUSION

Symmetry- and multiplet-resolved N 1*s* photoionization cross sections of the NO_2 near the N 1*s* shape resonance are obtained both theoretically and experimentally. We have confirmed theoretically and experimentally that the shape resonance appears only in the $A_1 \rightarrow B_2$ transition. It should be noted that the present study is the first experimental confirmation of this fact. The measured partial cross sections of the $^1A_1$ and $^3A_1$ channels are found to exhibit maxima at the photon energies of 416.3 and 415.9 eV, respectively, whereas the calculated maxima are at 414.34 and 416.25 eV, respectively. Although the present theory predicts most of the key features on the shape resonances in the N 1*s* photoionization region of NO_2, the attractive potential for the $^1A_1$ N $1s^{-1}$ state is very likely overestimated by the single-channel approximation. Additionally, *ab initio* RAS-SCF calculations on the N $1s^{-1}$ excited states have been presented and support the evidence that there are two separate shape resonances with significant oscillator strength in the main-line channels. A detailed account of the possible role played by interchannel coupling between the two $^1A_1$ and $^3A_1$ target states and possibly with additional excited target states (i.e., shake-up states) has been presented.

ACKNOWLEDGMENTS

The experiments were performed at SPring-8 with the approval of the program review committee, 2003A0581-NS1-np and 2004A0080-NSb-np. The work was partly supported by the Grants-in-Aid for Scientific Research from the Japan Society for Promotion of Science and by the Budget for Nuclear Research from Ministry of Education, Culture, Sports, Science and Technology, based on the screening and counseling by the Atomic Energy Commission. We are grateful to the staff of SPring-8. D.T. and R.R.L. also acknowledge the support of the Robert A. Welch Foundation of Houston (Grant No. A-1020) and the Texas A&M Supercomputing Facility. U.H. acknowledges the hospitality of Tohoku University.

[1] F. A. Gianturco, M. Guidotti, and U. Lamanna, J. Chem. Phys. **57**, 840 (1972).
[2] V. I. Nefedov, J. Struct. Chem. (USSR) **11**, 292 (1970).
[3] J. L. Dehmer, D. Dill, and A. C. Parr, in *Photophysics and Photochemistry in the Vacuum Ultraviolet*, edited by S. McGlynn, G. Findly, and R. Huebner (Reidel, Dordrecht, 1985).
[4] M. N. Piancastelli, J. Electron Spectrosc. Relat. Phenom. **100**, 167 (1999).
[5] J. W. Chamberlain and D. M. Hunter, *Theory of Planetary Atmospheres*, 2nd ed. (Academic, New York, 1987).
[6] R. S. Stolarski, Sci. Am. **258**, 30 (1988).

[7] W. H. E. Schwarz, T. C. Chang, and J. P. Connerade, Chem. Phys. Lett. **49**, 207 (1977).
[8] W. Zang, K. H. Sze, C. E. Brion, X. M. Tong, and J. M. Li, Chem. Phys. **140**, 265 (1990).
[9] X.-M. Tong and J.-M. Li, J. Phys. B **22**, 1531 (1989).
[10] T. Gejo, Y. Takata, T. Hatsui, M. Nagasono, H. Oji, N. Kosugi, and E. Shigemasa, Chem. Phys. **289**, 15 (2003).
[11] R. R. Lucchese, K. Takatsuka, and V. McKoy, Phys. Rep. **131**, 147 (1986).
[12] A. P. P. Natalense and R. R. Lucchese, J. Chem. Phys. **111**, 5344 (1999).
[13] F. A. Gianturco and A. K. Jain, Phys. Rep. **143**, 347 (1986).
[14] F. A. Gianturco, R. R. Lucchese, N. Sanna, and A. Talamo, in *Electron Collision with Molecules, Clusters and Surfaces*, edited by H. Ehrhardt and L. A. Morgan (Plenum, New York, 1994).
[15] Y. Muramatsu, K. Ueda, N. Saito, H. Chiba, M. Lavollée, A. Czasch, T. Weber, O. Jagutzki, H. Schmidt-Böcking, R. Moshammer, U. Becker, K. Kubozuka, and I. Koyano, Phys. Rev. Lett. **88**, 133002 (2002).
[16] N. Saito, K. Ueda, and I. Koyano, in *Dynamics of Photoionization and Photoexcitation of Molecules Probed by Multiple Coincidence Momentum Imaging*, edited by A. Bianconi, A. Marcelli, and N. L. Saini, AIP Conf. Proc. No. 652 (AIP, Melville, NY, 2003), p. 172.
[17] A. De Fanis, N. Saito, M. Machida, K. Okada, H. Chiba, A. Cassimi, R. Dörner, I. Koyano, and K. Ueda, Phys. Rev. A **69**, 022506 (2004).
[18] N. Saito, A. De Fanis, I. Koyano, and K. Ueda, Phys. Scr., T **T110**, 90 (2004).
[19] N. Saito, Y. Muramatsu, H. Chiba, K. Ueda, K. Kubozuka, I. Koyano, K. Okada, O. Jagutzki, A. Czasch, T. Weber, M. Hattass, H. Schmidt-Böcking, R. Moshammer, M. Lavollée, and U. Becker, J. Electron Spectrosc. Relat. Phenom. **141**, 183 (2004).
[20] D. A. Mistrov, A. De Fanis, M. Kitajima, M. Hoshino, H. Shindo, T. Tanaka, Y. Tamenori, H. Tanaka, A. A. Pavlychev, and K. Ueda, Phys. Rev. A **68**, 022508 (2003).
[21] M. Hoshino, T. Tanaka, M. Kitajima, H. Tanaka, A. De Fanis, A. A. Pavlychev, and K. Ueda, J. Phys. B **36**, L381 (2003).
[22] R. Sankari, M. Ehara, H. Nakatsuji, Y. Senba, K. Hosokawa, H. Yoshida, A. De Fanis, Y. Tamenori, S. Aksela, and K. Ueda, Chem. Phys. Lett. **380**, 647 (2003).
[23] D. L. Lynch and V. McKoy, Phys. Rev. A **30**, R1561 (1984).
[24] J. Schirmer, M. Braunstein, and V. McKoy, Phys. Rev. A **41**, 283 (1990).
[25] J. C. Slater, *The Self-Consistent Field for Molecules and Solids: Quantum Theory of Molecules and Solids* (McGraw-Hill, New York, 1974), Vol. 4.
[26] I. Wilhelmy and N. Rösch, Chem. Phys. **185**, 317 (1994).
[27] S. Motoki, J. Adachi, Y. Hikosaka, K. Ito, M. Sano, K. Soejima, A. Yagishita, G. Raseev, and N. A. Cherepkov, J. Phys. B **33**, 4193 (2000).
[28] N. A. Cherepkov, G. Raseev, J. Adachi, Y. Hikosaka, K. Ito, S. Motoki, M. Sano, K. Soejima, and A. Yagishita, J. Phys. B **33**, 4213 (2000).
[29] B. Zimmermann, K. Wang, and V. McKoy, Phys. Rev. A **67**, 042711 (2003).
[30] J. Adachi, K. Hosaka, S. Furuya, K. Soejima, M. Takahashi, A. Yagishita, S. K. Semenov, and N. A. Cherepkov, J. Electron Spectrosc. Relat. Phenom. **137**, 243 (2004).
[31] J. Adachi, K. Hosaka, S. Furuya, K. Soejima, M. Takahashi, A. Yagishita, S. K. Semenov, and N. A. Cherepkov, Phys. Rev. Lett. **91**, 163001 (2003).
[32] A. E. Hansen and T. D. Boumann, Chem. Phys. Lett. **45**, 326 (1977).
[33] D. Dill and J. L. Dehmer, J. Chem. Phys. **61**, 692 (1974).
[34] J. Siegel, D. Dill, and J. L. Dehmer, J. Chem. Phys. **64**, 3204 (1974).
[35] F. A. Gianturco and R. R. Lucchese, Int. Rev. Phys. Chem. **15**, 429 (1996).
[36] R. E. Stratmann and R. R. Lucchese, J. Chem. Phys. **97**, 6384 (1992).
[37] D. Toffoli, M. J. Simpson, and R. R. Lucchese, Phys. Rev. A **69**, 062712 (2004).
[38] F. A. Gianturco and R. R. Lucchese, J. Chem. Phys. **120**, 7446 (2004).
[39] R. D. Amos, A. Bernhardsson, A. Berning *et al.*, MOLPRO, a package of *ab initio* programs designed by H.-J. Werner and P. J. Knowles, version 2000.1 (University of Birmingham, Birmingham, 2000).
[40] G. Herzberg, *Molecular Spectra and Molecular Structure. III. Electronic Spectra and Electronic Structure of Polyatomic Molecules* (Van Nostrand Reinhold, New York, 1966).
[41] D. W. Davis, R. L. Martin, M. S. Banna, and D. A. Shirley, J. Chem. Phys. **59**, 4235 (1973).
[42] I. Koyano, M. Okuyama, E. Ishiguro, A. Hiraya, H. Ohashi, T. Kanashima, K. Ueda, I. H. Suzuki, and T. Ibuki, J. Synchrotron Radiat. **5**, 545 (1998).
[43] H. Ohashi, E. Ishiguro, Y. Tamenori, H. Kishimoto, M. Tanaka, M. Irie, T. Tanaka, and T. Ishikawa, Nucl. Instrum. Methods Phys. Res. A **467–468**, 529 (2001).
[44] T. Tanaka and H. Kitamura, Nucl. Instrum. Methods Phys. Res. A **364**, 368 (1995); J. Synchrotron Radiat. **3**, 47 (1996).
[45] H. Yoshida, Y. Senba, M. Morita, T. Goya, A. De Fanis, N. Saito, K. Ueda, Y. Tamenori, and H. Ohashi, AIP Conf. Proc. No. 705 (AIP, Melville, NY, 2004), p. 267.
[46] M. C. Hettrick and S. Bowyer, Appl. Opt. **22**, 3921 (1983).
[47] E. Ishiguro, H. Ohashi, L. Lu, W. Watari, M. Kamizato, and T. Ishikawa, J. Electron Spectrosc. Relat. Phenom. **101–103**, 979 (1999).
[48] H. Ohashi, E. Ishiguro, Y. Tamenori, H. Okumura, A. Hiraya, H. Yoshida, Y. Senba, K. Okada, N. Saito, I. H. Suzuki, K. Ueda, T. Ibuki, S. Nagaoka, I. Koyano, and T. Ishikawa, Nucl. Instrum. Methods Phys. Res. A **467–468**, 533 (2001).
[49] See http://www.roentdek.com for details on the detectors.
[50] Y. Shimizu, H. Ohashi, Y. Tamenori, Y. Muramatsu, H. Yoshida, K. Okada, N. Saito, H. Tanaka, I. Koyano, S. Shin, and K. Ueda, J. Electron Spectrosc. Relat. Phenom. **114–116**, 63 (2001).
[51] R. Curik, F. A. Gianturco, R. R. Lucchese, and N. Sanna, J. Phys. B **34**, 59 (2001).
[52] F. A. Gianturco and R. R. Lucchese, Phys. Rev. A **64**, 032706 (2001).
[53] P. van der Straten, R. Morgenstern, and A. Niehaus, Z. Phys. D: At., Mol. Clusters **8**, 35 (1988).
[54] R. E. Stratmann, R. W. Zurales, and R. R. Lucchese, J. Chem. Phys. **104**, 8989 (1996).
[55] A. Kivimäki, U. Hergenhahn, B. Kempgens, R. Hentges, M. N. Piancastelli, K. Maier, A. Rüdel, J. J. Tulkki, and A. M. Brad-

shaw, Phys. Rev. A **63**, 012716 (2001).
[56] M. Ya. Amusia, L. V. Chernysheva, S. T. Manson, A. M. Msezane, and V. Radojević, Phys. Rev. Lett. **88**, 093002 (2002).
[57] P. W. Langhoff, in *Resonances in Electron-Molecule Scattering, van der Waals Complexes and Reactive Chemical Dynamics*, edited by D. G. Truhlar (American Chemical Society, Washington, D.C., 1984), p. 113.